Supplemental Materials, Methods and Results:

Materials: Purified stroma free Hb was prepared from guinea pig RBC by washing with 10 mL volumes (x3) of cold 0.9% sodium chloride (NaCl) followed by centrifugation (6000 rpm x 30 min) and supernatant separation. Cells were lysed overnight in deionized water at 6°C. Stroma was separated from intracellular protein by centrifugation (6000 rpm x 30 min) and supernatant was loaded on a Superose 6 preparatory column (GE Healthcare) with phosphate buffer. Hb was collected, concentrated and buffer exchanged in 0.9% NaCl at 6 g/dL Hb. Mixed phenotype human Hp was fractionated from human plasma and provided as gift from (Benesis Corporation) as a 2% solution in phosphate buffered saline. This solution was further concentrated 5-fold using Centricon 10 kDa cut-off filters (Millipore Corp.) for co-infusion experiments. 25% human serum albumin was purchased from (Talecris Pharmaceuticals) and diluted to 5% with 0.9% normal saline. Hp standards isoforms 1-1 and 2-2 were purchased from (Sigma-Aldrich Chemical).

Animal and surgical preparation: Male Hartley guinea pigs were purchased from Charles Rivers Laboratories (Wilmington, MA) and acclimated for 1 week upon arrival to the FDA/Center for Biologics Evaluation and Research (CBER) animal care facility. All animals were fed normal diets throughout the acclimation period and weighed 350-450 g at the time of study. On days of surgery, guinea pigs were anesthetized via the i.p. route with a cocktail of ketamine HCl (100 mg/kg) and xylazine HCl (5 mg/kg) (Phoenix Scientific Inc.) and catheters were placed in left external jugular vein, right carotid artery and left femoral artery (for blood pressure monitoring) as reported in detail previously [19].

RBC deformability and analysis of free and intra cellular Hb: RBC deformability was measured by osmotic gradient ektacytometry using laser diffraction (RheoScan-D, rheomeditech). Briefly, 6 μl of stored blood were transferred to 600 μl of Poly Vinyl Pyrrolidone in phosphate buffered saline at a solution

osmolarity of 300 mOsm/L and subjected to several rotational speeds at 37°C with final shear stresses ranging from 0.3 to 30 Pa. Elongation index (EI) was calculated from the major (A) and minor (B) axes lengths as EI = (A-B)/(A+B) over the range of shear stresses. Data were plotted on a linear/log scale from 0.5 to 20 Pa. Samples were measured immediately after leukocyte reduction (day 0), day 14 (midpoint of storage) and day 28 (end of storage) with each time point representing the mean of n=3 measurements. Analysis of free- and intracellular hemoglobin content was performed on stored blood by UV-Visible spectrophotometry with subsequent multi-component analysis for oxy-Hb, deoxy-Hb, met-Hb and hemichrome as previously described [21]. Immediately after leukocyte reduction (day 0) and on days 7, 14, 21 and 28 of storage, samples (1 mL) were centrifuged at 6000 rpm for 10 minutes. Supernatant was separated from RBCs, volume was measured and then analyzed. RBCs were subjected to freezing and thawing followed by centrifugation at 10,000 rpm for 10 minutes to separate stroma from Hb, volume was measured, samples diluted and analyzed. The percentage of free Hb was calculated based on the (concentration of supernatant (free Hb)/concentration of RBC Hb)x100. Each time point is representative of the mean of n=3 measurements.

Hb measurements from transfused guinea pig plasma - Blood samples (0.1 mL) were obtained from guinea pigs transfused with new, old and old + Hp at baseline (time 0), 1, 2, 3, 4, 6, 8, 16 and 24 hours. Hb concentrations in plasma following blood transfusions were evaluated using a multicomponent analysis described previously [21].

Renal proteomics

iTRAQ labelling - The precipitated proteins were reconstituted in 20µl of dissolution buffer, 1µl of Denaturant and 4µl of 6M urea according to the iTRAQ manufacturer's instructions (Applied Biosystems, Framingham, USA). A total of 100 µg of protein was digested overnight at 37°C with trypsin (Promega, Madison, USA) in the ratio 1:10, trypsin to protein. Peptides (50µg) were

covalently modified for two hours with an isobaric tag reagent according to the following scheme: iTRAQ 114 (non treated, NT), iTRAQ 115 (new blood), iTRAQ 116 (old blood) and iTRAQ 117 (old blood-Hp). After combining the iTRAQ reagent labelled peptides, the reaction was stopped by adding phosphoric acid (pH 2-3).

SCX fractionation - Labelled peptides were fractionated by strong cation exchange liquid chromatography (SCX) using a Polysulfoethyl A 2.1 mm x 200 mm, 5 µm, 300 Å column (PolyLC, Columbia, MD). Solvent A was 10 mM potassium diphosphate, 25% acetonitrile (ACN), pH < 3.0, and solvent B was 10 mM potassium diphosphate, 350 mM potassium chloride, 25% ACN, pH < 3.0. The iTRAQ labeled peptides were diluted in a ratio 1:4 in solvent A and applied to the SCX column. After peptide mixture injection with a flow rate of for min peptides were fractionated during a 50 min linear gradient of solvent B (0 – 100%) at a flow rate of 0.3 ml/min. For each HPLC run, 27 fractions were collected at each peak and partially evaporated to remove ACN on a speed vacuum. The collected fractions were resolved in 5% ACN, 0.1% Trifluoroacetic acid (TFA), combined to 9 pools and desalted with Sep Pak C_{18} cartridges (Waters, Milford, MA, USA). The 9 labelled sample pools were dried in a vacuum concentrator and reconstituted in 20 µl of 3% (v/v) acetonitrile/0.2% formic acid. All procedures were repeated with the kidney lysates of four independent animals with random iTRAQ experiment group assignment.

LTQ-Orbitrap measurements - LC-MSMS was performed on a LTQ-Orbitrap Velos mass spectrometer (Thermo Scientific, Bremen, Germany) coupled to an Eksigent nano LC system (Eksigent Technologies).

Solvent composition at the two channels was 0.2% formic acid, 1% acetonitrile for channel A and 0.2% formic acid, 100% acetonitrile for channel B. Peptides were loaded on a self-made tip column (75 µm × 80 mm) packed with reverse

phase C18 material (AQ, 3 µm 200 Å, Bischoff GmbH, Leonberg, Germany) and eluted with a flow rate of 250 nl per min by a gradient from 2 to 30% B in 62 min, 30-50% B in 3 min and 50-98%B in 2 min.

Full-scan MS spectra (300−1700 m/z) were acquired in the FT-Orbitrap with a resolution of 60 000 at 400 m/z after accumulation to a target value of 1E6. iTRAQ labelled peptides were following analysed by eight sequential data-dependent CID and HCD MS/MS fragmentation of the same precursor. The signal threshold necessary to trigger the CID and HCD fragmentation was set, respectevely, to 1000 and 4000. CID spectra were recorded in the ion trap with a target value of 5E3, using a normalized collision energy of 35%, an activation time of 10 ms and a Q value of 0.25. HCD fragmentation ions including reporter ions were detected in the Orbitrap with a resolution of 7500 at 400 m/z, with a target value of 3e4, using a normalized collision energy of 45% and 30 ms activation time.

For all experiments charge state screening was enabled and singly charge states were rejected. The precursor masses already selected for MS/MS were excluded for further selection for 60 s and the exclusion window was set to 20 ppm. The size of the exclusion list was set to a maximum of 500 entries. The instrument was calibrated externally according to the manufacturer's instructions. The samples were acquired using internal lock mass calibration on m/z 429.088735 and 445.120025.

Peptide and protein identification and quantification by database searching - Raw spectra were processed with Mascot Distiller 2.2 (Matrix Science, London, UK) and protein identification was performed using Mascot Version 2.2.0 (Matrix Science, London, UK) as the search engine. Mascot generic files were searched against a NCBI guinea pig protein sequence database (downloaded 04.29.2009). The following search settings were used: maximum missed cleavages: 1; maximum number of signals per spectrum: 55; peptide mass tolerance: 8 ppm, fragment ion tolerance: 0.8 Da. iTRAQ4plex reagent labelling of lysine and of the

N-terminal amino group of peptides and methyl methanthiosulfonate (MMTS) derivatization of cysteine were specified as fixed modifications, oxidation on methionine as variable modification. Quantitative data analysis and normalization were performed with Scaffold Software 3 Q+ (Proteome Software Inc, Portland, OR). At the chosen levels of peptide and protein assignment stringencies the calculated false discovery rates (FDR) were <1% at a peptide and <5% at the protein identification level.

Tissue pathology and Hb exposure: Gross morphology of kidney transverse cuts were documented photographically at the time of tissue harvesting (24 hours post transfusion). Tissues (kidney and aortic arch) were collected for freezing (liquid nitrogen to -80°C) and 10% formalin for 24 hours then transfer to 70% isopropanol. Fixed tissues were embedded in paraffin and 5 μm sections were prepared, dewaxed in Safeclear II, rehydrated in graded ethanol and stained with hematoxylin and eosin. *Non-heme iron histochemistry* - Sections were incubated with Perls iron reagent containing 5% potassium ferrocyanide and 2% hydrochloric acid for 45 minutes at room temperature and rinsed in deionized water. Sections were then incubated with 0.3% hydrogen peroxide and 0.01 M sodium azide in methanol for 30 minutes at room temperature. All sections were then rinsed in 0.1 M phosphate buffer, pH 7.4, incubated with diaminobenzidine (SigmaFast™ DAB, Sigma) for three minutes, washed in deionized water, and lightly counterstained with Gill's II hematoxylin. *Renal iron measurement (ferrozine assay)* – Renal cortical and medullary tissue (100 mg) was homogenized in double deionized water (1:10 w/v) according to previously described methodology [46]. *Globin chain deposition (Okajima staining)* - Sections were incubated with 100 ml 5% Alizarin Red + 50ml 10% Phosphomolybdic acid for 1 hour, washed in deionized water, and lightly counterstained with Gill's II hematoxylin. Morphometric analysis/*Tissue scoring* - Tissue was identified as normal, abnormal (partial loss of intima and media vascular nuclei as well as loss of normal distribution of vascular smooth muscle cells) or necrotic (regions of coagulation marked by complete loss of nuclei and vascular smooth muscle

cellular morphology). *Nrf-2 and HO-1 western blotting* - Renal cortical and medullary tissue (100 mg) was homogenized in 50 mM Tris, pH 7.6, 150mM NaCl, 1% IgePal-630, 1 mM EDTA, 0.25% sodium deoxycholate) with a protease inhibitor cocktail and incubated with a primary antibody to Nrf-2 (1:1000) (mouse monoclonal anti-Nrf-2, cat# 81342, Santa Cruz Biotechnology) or HO-1 (1:5000) (rabbit polyclonal anti-HO-1, cat# SPA-894, Assay Designs) overnight and then incubated with a relevant HRP-conjugated secondary antibody for 1 hour. *Immunofluorescence* – Aorta and kidney paraffin sections were dewaxed and rehydrated. Sections were blocked in PBS-T with 5% goat serum and 0.25% Triton-X for 1 h at room temperature followed by overnight incubation with rabbit polyclonal anti-HO1 (1:400) at 4 °C. Sections were rinsed and incubated with a relevant Alexa-Fluor 488-conjugated secondary antibody for 1 hr at room temperature. For aorta, sections were additionally incubated with mouse anti-CD163 (1:100) (mouse monoclonal anti-CD163, clone EDHu-1, AbD Serotec) at 4°C overnight, rinsed and incubated with Alexa-Fluor 555-conjugated secondary antibody for 1 hr at room temperature. For kidney, a rabbit polyclonal anti-Nrf-2 was used (1:1000) and incubated overnight. Sections were rinsed and incubated with a relevant Alexa-Fluor 488-conjugated secondary antibody for 1 hr at room temperature. Nuclei were counterstained with Hoechst 33342. All images were acquired using an Olympus IX71 inverted microscope equipped with an Olympus DP70 digital camera. *Serum creatinine* – Measurements were made on whole blood (150 μl) obtained at baseline and at study termination (24 hours) using an i-STAT analyzer (Abaxis Diagnotics) with creatinine cartridges (lot # 10250).

Non-heme iron histochemistry – Liver and spleen Sections were incubated with Perls iron reagent containing 5% potassium ferrocyanide and 2% hydrochloric acid for 45 minutes at room temperature and rinsed in deionized water. Sections were then incubated with 0.3% hydrogen peroxide and 0.01 M sodium azide in methanol for 30 minutes at room temperature. All sections were then rinsed in 0.1 M phosphate buffer, pH 7.4, incubated with diaminobenzidine (SigmaFast™ DAB, Sigma) for three minute, washed in deionized water, and lightly

counterstained with Gill's II hematoxylin. All images were acquired using an Olympus IX71 inverted microscope equipped with an Olympus DP70 digital camera.

Immunofluorescence –Liver and spleen were performed on praffin-embedded slides that were dewaxed and rehydrated. Sections were blocked in PBS-T with 5% goat serum and 0.25% Triton-X for 1 h at room temperature followed by overnight incubation with rabbit polyclonal anti-HO1 (1:400) (rabbit polyclonal anti-HO-1, cat# SPA-894, Assay Designs) at 4 °C. Sections were rinsed and incubated with a relevant Alexa-Fluor 488-conjugated secondary antibody for 1 hr at room temperature. Nuclei were counterstained with Hoechst 33342. All images were acquired using an Olympus IX71 inverted microscope equipped with an Olympus DP70 digital camera.

In vitro oxygenation: To evaluate the potential contribution of decreased tissue oxygenation or hypoxia induced by older storage blood in vitro and in vivo measures of tissue oxygenation were studied. Oxygen equilibrium curves for new and old blood were obtained using a Hemox analyzer (TCS Scientific) and Oxygen dissociation kinetics from RBCs and CO binding to deoxy RBCs were measured in an Applied Photophysics SF-17 microvolume stopped-flow instrument with a dead time of approximately 1.5 ms as previously described (1).

In vivo oxygenation: Arterial and venous blood gases were measured at baseline and 24 hours post transfusion using an i-STAT analyzer (Abaxis Diagnositics, Union City, CA) with CG4+ blood gas cartridges (lot # R10259). A positive control for Hypoxia inducible factor-1 (HIF-1α) stabilization was evaluated in separate groups of animals designated to be euthanized at 8 and 24 hour were transfused with human serum albumin 5% (Talecris, Research Triangle Park, North Carolina) at 80% of their blood volume. Additionally, hypoxia treated HEK293 cells were evaluated as positive controls for HIF-1α stabilization in kidney. Cells were subjected to 1% oxygen over a four hour period. Control

cells and kidneys as well as treatment animal kidneys (100–200 mg) were homogenized in ice cold RIPA lysis buffer (Millipore, Temecula, CA) containing protease inhibitors (Roche, Germany). Samples were separated on 4-12% Tris-glycine (TG) gels (Invitrogen, Inc, Carlsbad, CA) and transferred to nitrocellulose membranes (Bio-rad Lab, Hercules, CA). The membranes were blocked in Tris-buffered saline with 0.1% Tween 20 (TBS-T) containing 5% nonfat dry milk and incubated with primary antibodies against to HIF-1α (R&D Systems, Minneapolis, MN), and β-action (Santa Cruz Biotechnology, Inc., Santa Cruz, CA). After multiple washes in TBS-T, the membranes were incubated with appropriate HRP-conjugated secondary antibodies and detected bands using the ECL Plus chemiluminescence kit (Amersham, Arlington Heights, IL). Densitometry analysis was performed using NIH ImageJ software. Equal protein loading was verified by stripping and reprobing membranes for β-actin.

Haptoglobin dose response: A separate study was conducted to determine the biological dose response of Hp at 100, 300 and 900 mg when administered with old blood. The purpose of this study was to evaluate if there was a dose dependent effect of Hp on NO and Hb interactions, plasma NO metabolites, MAP and Hb plasma concentration following old blood and differing Hp doses and aortic root injury.

Stopped flow kinetics: The kinetics of NO-induce oxidation of oxyHb in the presence and absence of Hp were carried in the stopped-flow instrument. Hb solutions equilibrated in air were mixed with the anaerobic solutions of NO in the stopped-flow instrument, and the absorbance changes of the reaction were followed 420 nm. The concentrations of reaction solutions were kept low for Hb (1 μM) and NO (≤ 25 μM) to allow the measurement of the fast reaction, and the NO concentration was in excess versus Hb to maintain the pseudo-first order conditions. Reactions of ferric (met) Hbs with NO were measured in the stopped-flow as previously described (2). Hb solutions (1 μM in heme) were mixed with increasing concentration of NO (up to 75 μM) to start the reaction and the

absorbance changes were monitored at 420 nm. Multiple kinetic traces were averaged and nonlinear least-squares curve fitted to exponential equations to obtain reaction rate constants.

NO metabolite measurements: Analysis of plasma samples for nitrite (NO_2^-) and nitrate (NO_3^-) was evaluated immediately from plasma collected at baseline, 1, 2,3,4,6,8,12,16 and 24 hours after transfusion with old blood + 100, 300 and 900 mg of haptoglobin (n=4/group). Blood was centrifuged at 500 g, plasma was obtained and 10 μL was mixed with 20 μL of methanol in an eppendorf tube. Samples were vortexed (10 seconds) and centrifuged at 10,000 G for 10 minutes. 20 μL of supernatant was injected on to a NO-Pak (4.6 mm x 50 mm) polymer gel column (EiCom Corp., San Diego, CA). Carrier and reactor solutions were prepared according to manufacturer instructions and run as mobile phase at a rate of 0.33 mL/min. Actual plasma values for NO_2^- and NO_3^- were obtained from a prepared standard curve and added together to provide NOx values ($NO_2^- + NO_3^-$).

Plasma hemoglobin measurements: Hb concentrations in plasma following blood transfusions were evaluated using a multicomponent analysis described previously (3). Corresponding plasma Hb values were used to plot Hb concentration versus NOx and regression analysis was performed in SigmaPlot 11.0 (Systat Inc., Chicago, IL).

Morphometric analysis/*Tissue scoring* - Tissue was identified as normal, abnormal (partial loss of intima and media vascular nuclei as well as loss of normal distribution of vascular smooth muscle cells) or necrotic (regions of coagulation marked by complete loss of nuclei and vascular smooth muscle cellular morphology). Collagen was quantified using Image J software (NIH, Bethesda, MD). Quantitation of Masson Trichrome-stained tissue is presented as means of % collagen per total section area ± sem (n=3-4 animal per group).

Blood washing – Stored RBCs were washed 6 times with phosphate buffered saline (PBS). Each wash was with 2 fold the volume of RBCs followed by centrifugation at 400g. After the final wash RBCs were resuspended in 5% albumin (Talecris, Research triangle park, NC) to a hematocrit of 40%. These cells were not stored further and immediately transfused.

In vitro nitric oxide (NO) consumption assay - Constant NO levels were generated in a closed stirred 2ml glass chamber by decay of the long half-life NO donor DETA NONOate (Enzo Life Sciences, Switzerland). The reaction was performed with 5mM DETA NONOate in essentially anaerobic PBS (pH 7.4) at 23°. NO was monitored at a 1/s recording rate with a Clark-type NO microsensor (Unisense, Denmark). Plasma samples were injected into the closed reaction system with a gas-tight Hamilton syringe as 3 consecutive identical boluses at 30s intervals. Data were recorded with SensorTrace basic software (Unisense, Denmark). Statistical analysis of replicate measurements was performed with GraphPad Prism Software Version 5.01.

Supplemental Results:

Old blood transfusion related tissue damage is not caused by tissue hypoxia To rule out the potential for decreased tissue oxygenation as a causative factor in the observed tissue injury, we studied *in vitro* oxygen equilibrium curves of new and old blood prior to transfusion as well as stopped flow kinetic parameters to determine both oxygen on and off rates of new and old blood (supplemental Figure 2 A-C). Small, but statistically significant differences were observed in the oxygen saturation properties of new blood (p50 = 25 ± 0.51 mmHg) versus old blood (p50 = 19 ± 0.14) that are consistent with depletion of 2,3-DPG in stored RBCs. Additionally, minimal differences were seen in fast kinetic parameters such as oxygen on- and off-rates of new versus old blood. Arterial and venous pO_2 levels as well as a marker of tissue oxygenation were evaluated. While no group differences were seen in arterial pO_2, we observed a slightly decreased venous pO_2 in the old blood transfused animals at 24 h post-transfusion compared to the new blood group. Comparable venous pO_2 differences were also noted in the old blood + Hp transfused animals. Furthermore, stabilization of hypoxia inducible factor-1 (HIF-1) as evaluated by western blotting in kidney tissue at 8 and 24 hours after transfusion indicated no time dependent tissue hypoxia (Supplemental Figure 3). Collectively, these data suggest that transfusion-induced oxygen debt and/or tissue hypoxia are not causative factors underlying these observations. Moreover, the main pathologic changes observed with old blood were effectively prevented by Hp co-infusion, and it is therefore unlikely that tissue hypoxia could account for old blood transfusion associated pathologies.

Supplemental Figure Legends:

S. Figure 1. Hepatic and splenic HO-1 and iron distribution following transfusion. **(A)** Immunofluorescence of liver HO-1 was absent in non treated (NT) and new blood transfused animals at 24 hours post transfusion (200x). **(B)** Shows Perl's iron staining in these tissues with reactivity in macrophages (200x) (**B** old blood and **B** old blood + Hp insets 400x). **(C)** Immunofluorescence of spleen HO-1 shows less reactivity in NT and new blood transfused animals at 24 hours post transfusion (200x, inset 400x). **(D)** shows Perl's iron staining in these tissues with visually greater reactivity in the red pulp of old blood and old blood + Hp compared to NT and new blood transfused animals (200x, inset 400x). Scale bars (1 cm) = 50 μm A, B, C, D and insets 25 μm.

S. Figure 2. *In vitro* Oxygen interaction with 2 and 28 day old blood cells prior to transfusion. **(A)** shows the oxygen equilibrium curves for 2 day (new blood) guinea pig blood and 28 day (old blood). Statistically significant ($p<0.05$) differences were observed in the P50 values of the two storage times. Stopped-flow kinetics of oxygen dissociation and ligand binding of guinea pig red blood cells. The kinetics of oxygen dissociation and CO association of stored guinea pig RBCs were measured in an Applied Photophysics stopped-flow at 25°C in 0.05M k phosphate buffer, pH 7.4. **(B)** The kinetic trace of oxygen dissociation shows the time-dependent increase in absorbance at wavelength of 437.5 nm. The solid line is the nonlinear least-squares fit to the single exponential increase equation. **(C)** The representative trace of CO binding shows the time-dependent decrease in absorbance at wavelength of 437.5 nm. The solid line is the nonlinear least-squares fit to the single exponential decay equation.

S. Figure 3. *In vivo* tissue oxygen status post transfusion. **(A)** shows the arterial pO_2 values prior to transfusion and at 24 hours post transfusion. Mean values are indicated in red. Overall mean values were not statistically different between any of the groups or their basal values. **(B)** shows venous pO_2 values prior to

transfusion and at 24 hours post transfusion. Mean values are indicated in red. Overall mean values were lower ($p<0.05$) in the old blood transfused animals, but not in animals transfused with old blood + Hp. The effect of these observations on renal tissue as determined by hypoxia inducible factor (HIF-1) stabilization shown in **(C)** were evaluated in kidney at 8 and 24 hours post transfusion. The positive control for HIF stabilization in kidney tissue was obtained from kidney lysates from animals transfused with human serum albumin at 80% of their blood volume (control 1). The lower band at approximately 110 kDa represents HIF-1α. All other bands represent non-specific immunoreactivity. Lysates of HEK293 cells subjected to 4 hours of hypoxia (2% oxygen) were used as a secondary control (control 2). Clearly no transfusion related HIF stabilization is observed at 8 or 24 hours. Control 1, representative of anemic/hypoxic animals demonstrates temporal HIF stabilization at 8 hours only.

S. Figure 4. The deposition of vascular tissue iron, HO-1, CD163 and nuclei merge of **(A)** new blood, **(B)** old blood and **(C)** old blood + Hp (all 200x). No exposure to heme/Hb is indicated following new blood transfusion, however increased exposure is indicated in the adventitia, connective tissue and vaso vasorum of old blood ± Hp transfused animals. Scale bars (1 cm) = 50 μm A, B, C.

S. Figure 5. Nitric Oxide interactions. **(A)** Ex-vivo NO consumption of plasma obtained at 1 hour post transfusion (top) and 24 hours post transfusion (bottom). Arrows indicate identical serial 10 μl injections of plasma samples into the reaction chamber with the of the long half-life NO donor DETA NONOate. The ex-vivo NO consumption of baseline plasma (black trace) and plasma samples obtained at 1-2 hours following old blood + Hp transfusion (blue trace) and without Hp (red trace) are shown in the top panel. The Hb depleted 24 hour old blood transfusion plasma (black trace), 24 hour old blood transfusion + Hp plasmas are shown in the bottom panel (n=3-5). **(B)** plasma NO metabolites (NO_x, NO_2^- + NO_3^-) are plotted over a 24 hour time course in plasma as mean ±

sem after old blood (plus infusion of ○ 100 mg, • 300 mg and • 900 mg doses of haptoglobin) (n=3 guinea pigs per group), no within group or between group differences were detected. **(C)** Blood pressure response to old blood (plus infusion of ○ 100 mg, • 300 mg and • 900 mg doses of haptoglobin) (n=3 guinea pigs per group). Significant ($p<0.05$) differences in blood pressure response detected in the first 2 hours after transfusion the 100 mg, 300 mg and 900 mg of haptoglobin. **(D)** The reactions of NO and oxyHb (1 μM heme, before mixing) in the presence and absence of haptoglobin were measured, and the observed pseudo-first-order rate constants were plotted versus NO concentrations. Bimolecular rate constants of NO-induced oxidation reaction of oxyHb with (•) and without (•) haptoglobin were derived from the slopes of the plot and reported in the results section of the main manuscript. **(E)** The observed pseudo-first-order rate constants of the fast and slow phases were plotted versus NO concentrations for the reactions of NO with 1 μM ferric Hb. Bimolecular rate constants of NO reaction with ferric Hb in the presence (• for k_1 and ■ for k_2) and absence (•**)** for k_1 and ■ for k_2) of haptoglobin were derived from the slopes of the plot and reported in the results section of the main manuscript.

S. Figure 6. Aortic root changes with increasing haptoglobin dose. **(A)** shows representative images of the aortic root at 100x magnification. **(B)** Shows the morphological evaluation of % aortic root demonstrating normal, abnormal and necrotic changes (n=3-5 animals/treatment). Significant ($p<0.05$) differences were observed between NT (#) and new blood (∗) and the old blood (0 mg haptoglobin) and the old blood (100 mg) comparing % necrosis. Similarly, Significant ($p<0.05$) differences were observed between NT (#) and new blood (∗) compared to % abnormal tissue in all the haptoglobin dosing groups. Scale bars (1 cm) = 100 μm for all images in A.

References

1. Fronticelli, C., Bucci, E., and Orth, C. 1984. Solvent regulation of oxygen affinity in hemoglobin. Sensitivity of bovine hemoglobin to chloride ions. *J Biol Chem* 259:10841-10844.
2. Alayash, A.I., Fratantoni, J.C., Bonaventura, C., Bonaventura, J., and Cashon, R.E. 1993. Nitric oxide binding to human ferrihemoglobins cross-linked between either alpha or beta subunits. *Arch Biochem Biophys* 303:332-338.
3. Winterbourn, C.C., editor. 1985. *Reactions of superoxide with hemoglobin*. Boca Raton, Florida: CRC Press. 137-141 pp.

Supplemental Figure 1

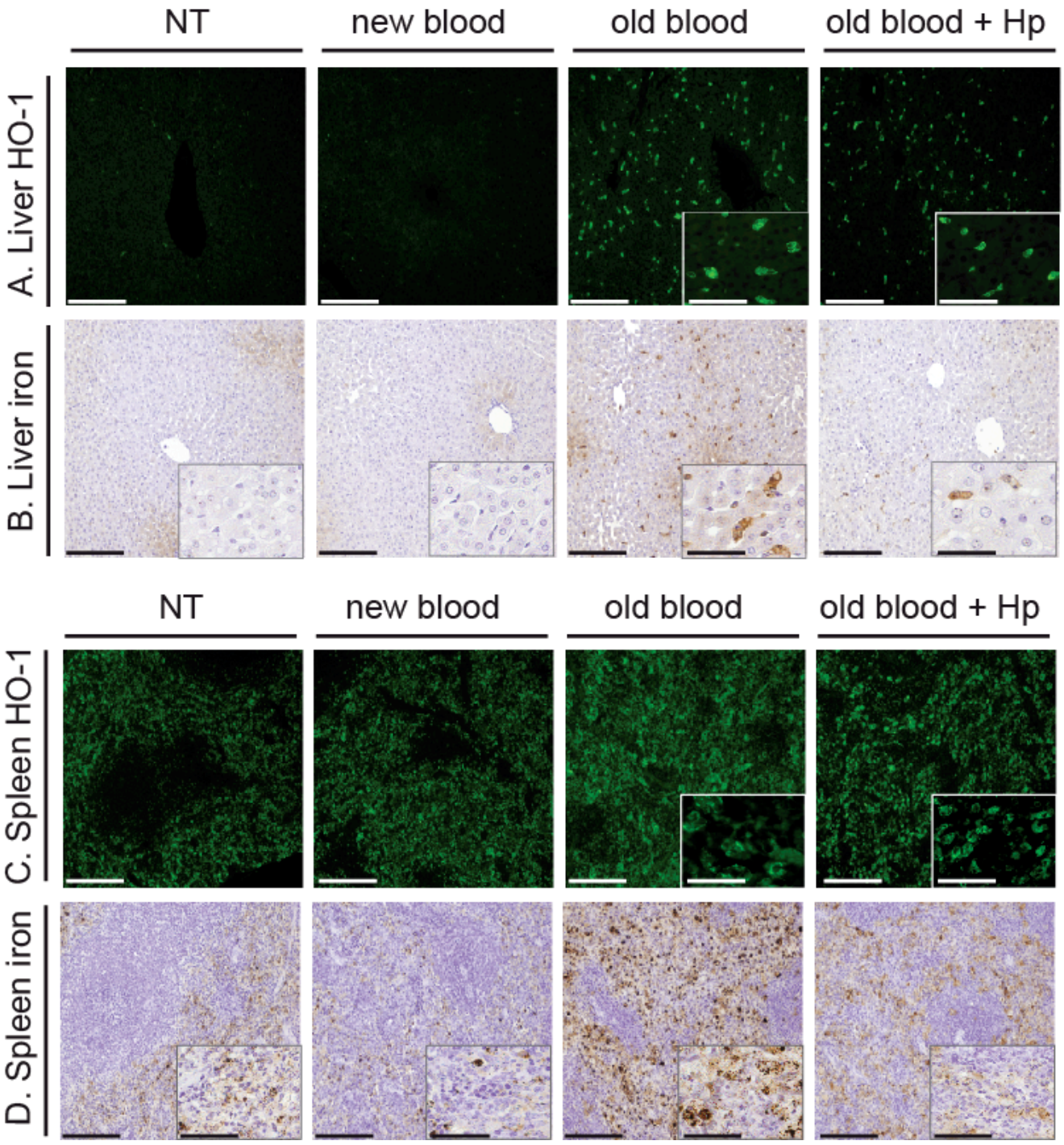

Supplemental Figure 2

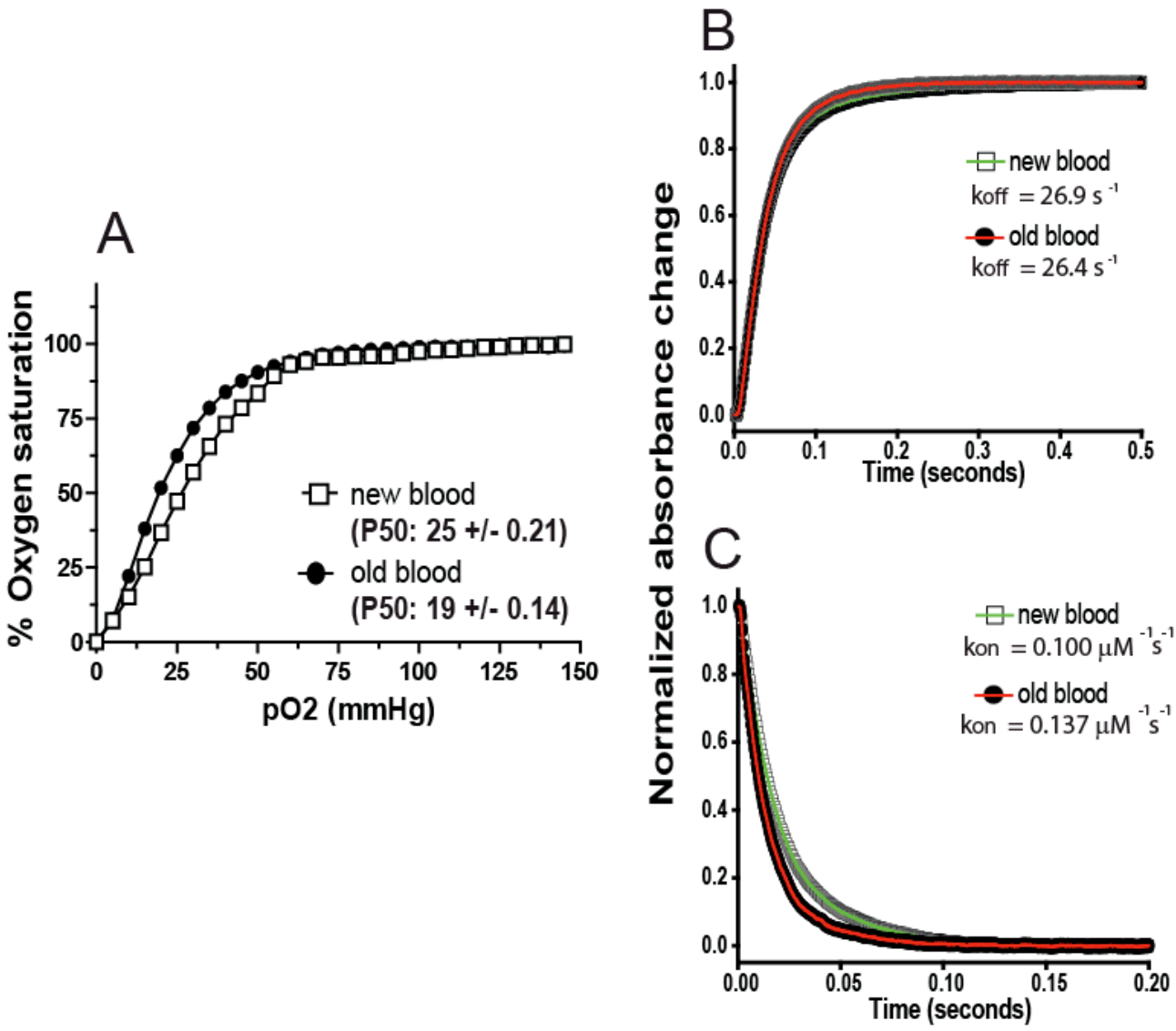

Supplemental Figure 3

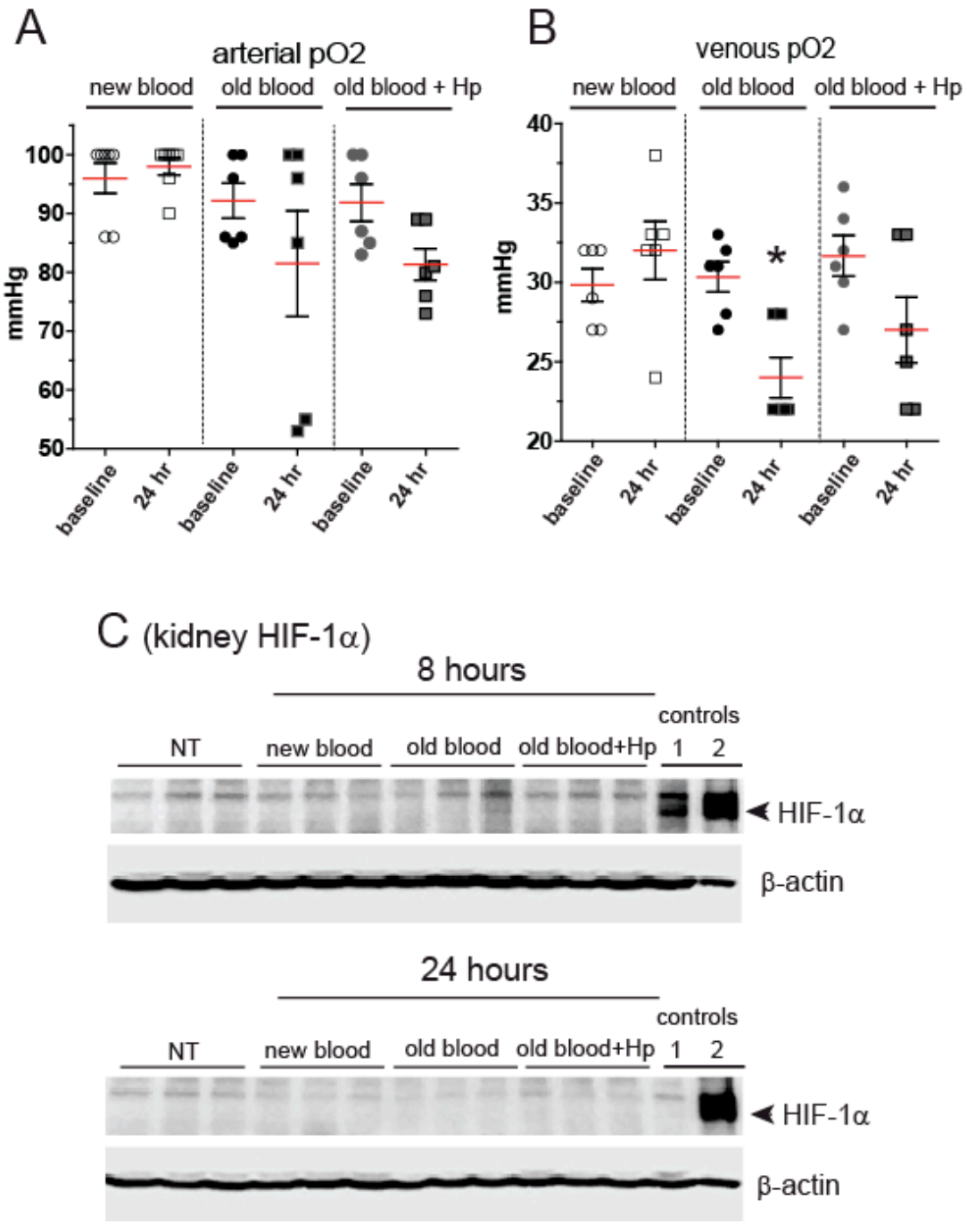

Supplemental Figure 4

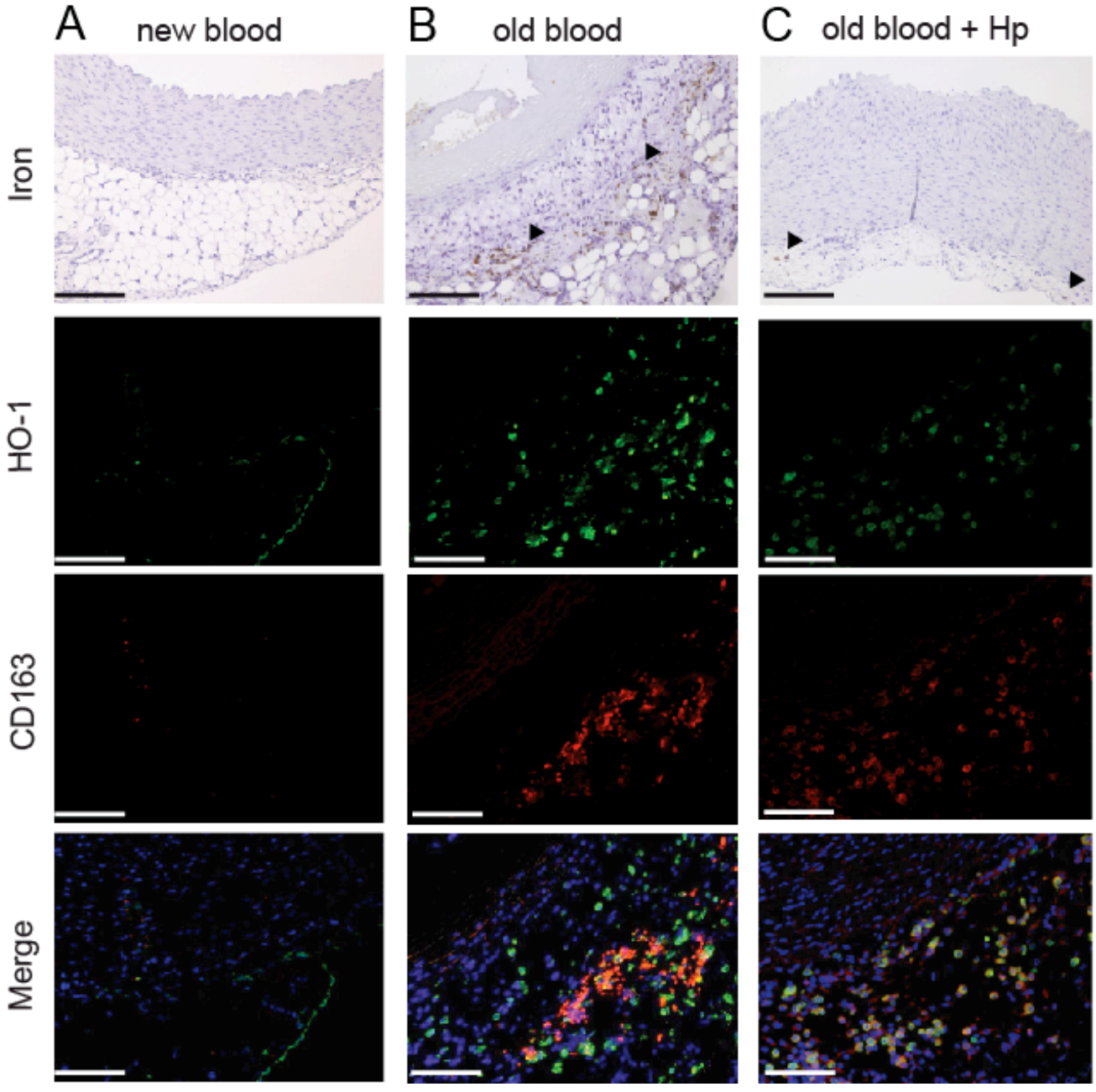

Supplemental Figure 5

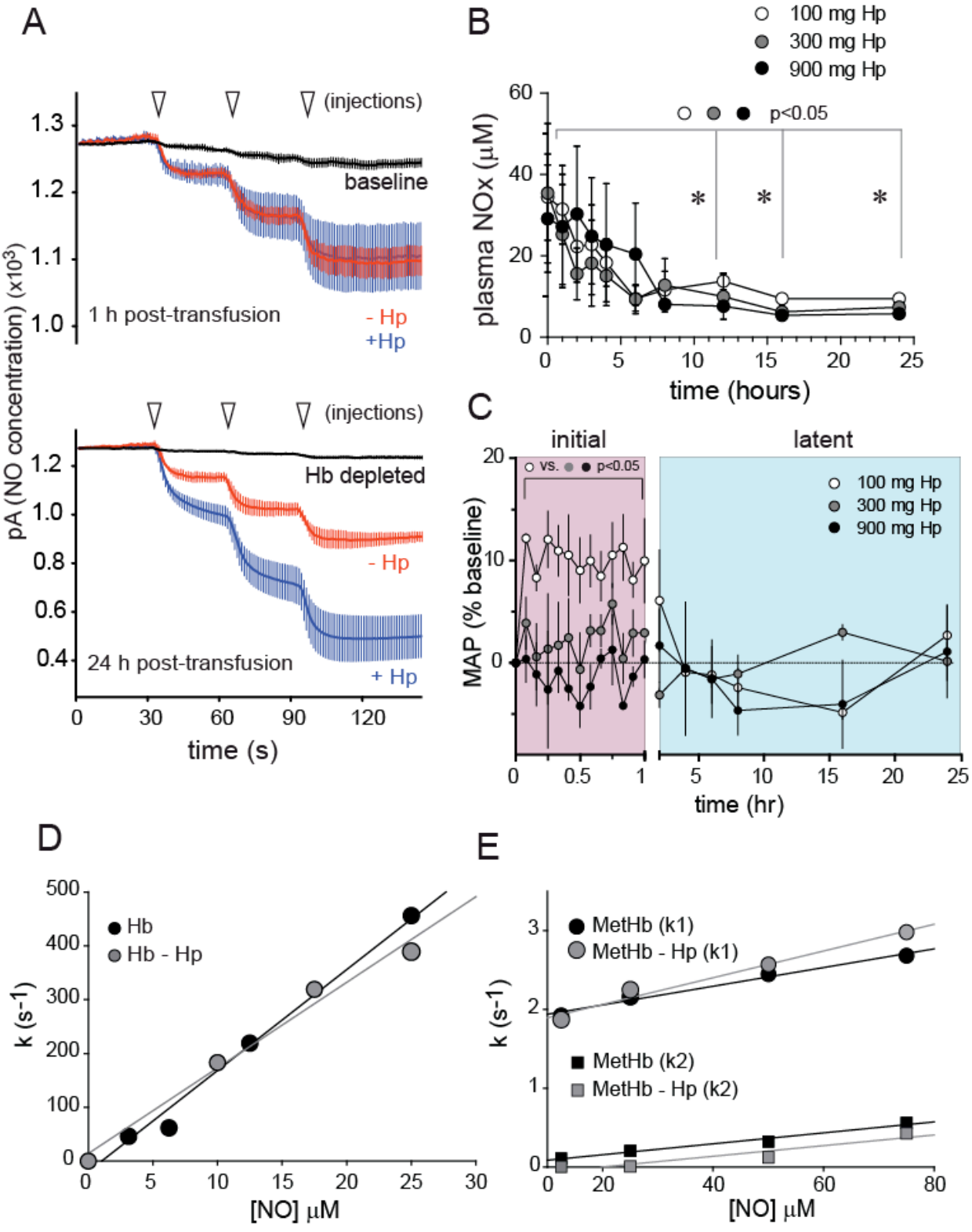

Supplemental Figure 6